J Appl Electrochem (2010) 40:1957–1966
DOI 10.1007/s10800-010-0172-0

ORIGINAL PAPER

Experimental investigation of cell design for the electrolysis of iron oxide suspensions in alkaline electrolyte

Antoine Allanore · H. Lavelaine · J. P. Birat · G. Valentin · F. Lapicque

Received: 18 December 2009 / Accepted: 4 July 2010 / Published online: 14 July 2010

Abstract Following feasibility studies of iron production by electrolytic reduction of hematite particles suspended in a strong alkaline medium, this article concerns the use of engineering methods to investigate the performance of various cell configurations, in view to designing larger processes: a horizontal flow cell with parallel electrodes and two rotating cylindrical electrodes were used for this purpose. The performance was analyzed in terms of current efficiency at 0.1 A cm^{-2} and deposit morphology. The results reveal a negligible role of the mass transfer of Fe (+III) ions from the bulk electrolyte on the process efficiency, as formerly suggested in reaction mechanism studies. Conventional ion-mass transfer theory is therefore not applicable and another approach is proposed. Dispersed phase transport processes, more precisely the mechanical forces acting on both the 10 μm ore particles and the evolved oxygen bubbles, can quantitatively and qualitatively explain the cells performance. The configuration with the external rotating cathode allows both efficient contacts of the particles with the cathode and rapid removal of the produced gas phase; however the two rotating electrode devices are subject to appreciable ohmic losses due to the current lead system. The parallel plate configuration, with the cathode at the bottom appears as the best configuration for the deposition which can be achieved with low energy consumption.

A. Allanore (✉) · H. Lavelaine · J. P. Birat
ArcelorMittal Maizières Research SA, Voie Romaine,
57280 Maizieres les Metz, France
e-mail: allanore.antoine@gmail.com

A. Allanore · G. Valentin · F. Lapicque
Laboratoire de Réactions et Génie des Procédés (LRGP),
CNRS-Nancy Université, BP 20451,
54001 Nancy Cedex, France

Keywords Hematite electrolysis · Iron production · Cell configuration · Particles deposition · Suspension electrolysis · Metal deposition

1 Introduction

Electrolysis is one of the breakthrough techniques studied in the search of Ultra Low CO_2 Steelmaking Processes [1]. One possible process is the low temperature alkaline-based electrolysis of hematite particles in suspension (http://www.ulcos.org) [2]. Recently, the unusual reaction mode of solid iron ore particles in alkaline electrolyte has been investigated [3], revealing the specificity of the electrochemical mechanism. Iron oxide particles can react in contact with the cathode in a solid-state-like mode, allowing direct conversion to iron metal. Surprisingly enough for the electrochemist community, the role of the iron ions from the bulk of the electrolyte on the metal deposition reaction has been shown as negligible in mechanism studies [2]. Altogether, these results provide a better understanding of the electroreduction and justify the development and successes obtained in the very first electrowinning experiments [4, 5]. However, concerning the iron oxide reactant transfer to the cathode, experimental and theoretical results are scarce. A recent study [6] has proved that hematite particles in 50 wt% NaOH–H_2O can easily adsorb on iron, suggesting that the contact time of the particles does not control the overall rate of the process.

Currently, the microscopic aspects of the cathode reaction are then relatively well understood, so that studies to be conducted at a larger scale could be more easily interpreted or modeled with a view to designing a pilot cell. The study presented in this article is, therefore, related to the

electrochemical engineering aspect of this process, evaluated on the basis of experimental devices.

In this field, recent small-scale metal deposits obtained on the classical rotating disc electrode configuration [7] have confirmed the interesting purity of the iron metal produced from iron oxide particles in alkaline media. Moreover, high current densities together with high efficiency of metal deposition have been obtained.

Nevertheless, the knowledge of the key engineering parameters to guarantee a successful scale-up of this process is still missing. One important issue to design the most suitable electrolysis cell configuration is the role of hydrodynamics in the cell, and the possible control of performance related to mass-transfer phenomena [8]. Another important aspect which has not been studied yet, is the handling of the oxygen gas produced at the anode. Indeed, no reports on iron electrowinning in alkaline electrolytes with same anode and cathode surface area have ever been published. The issues related to the large-scale application of this process, especially in terms of energy and reactant/product handling, therefore need further investigations.

This article is dedicated to the study of iron electrowinning from a suspension of hematite particles in strong alkaline solutions in three electrolysis configurations which are representative of large scale electrolysis cells. The first objective is to determine which hydrodynamic phenomena are keys for the production of compact deposits—as needed to develop a large scale process with metal deposit handling—with high faradaic efficiency, which is a prerequisite for low energy consumption.

Adopting conventional electrochemical engineering theory as first approach, the process features are evaluated in various configurations which provide various mass-transfer rates, which were estimated using the diffusive-convection theory. Cell voltage variation in these different configurations is also evaluated, as a parameter of primary importance to validate the interest of this process in terms of energy consumption. The second objective is to evaluate the role of the oxygen production and of flow conditions on the energy requirement: both the gas phase produced at the anode and the solid particles are a barrier to electric conduction in the cell and deserve a dedicated configuration. Finally, the use of large current densities is expected to help in technological choice for preliminary design of a dedicated electrolysis cell.

2 Experimental

2.1 Reactors

Three types of reactors frequently encountered in electrodeposition processes have been used as shown in Fig. 1, which dimensions and features are compiled in Table 1.

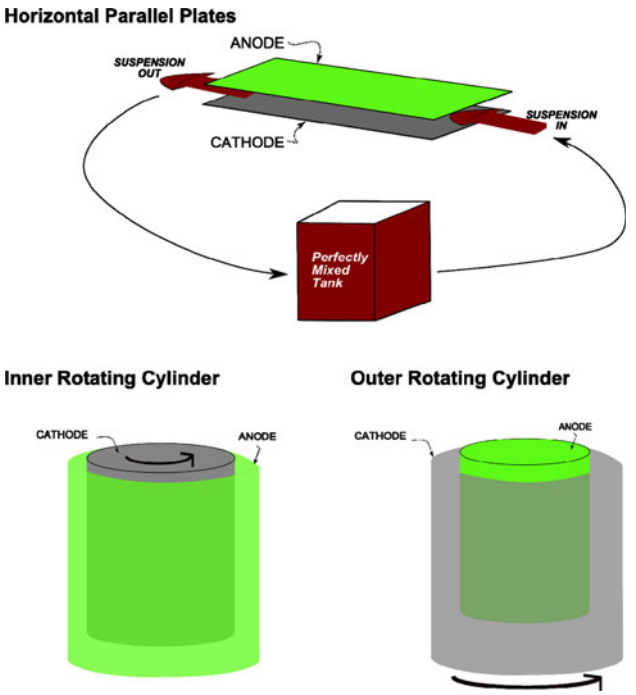

Fig. 1 Principle of the three experimentally studied configurations

Table 1 Electrolysis cell features

	Parallel plates (PP)	Inner rotating cylinder electrode (IRCE)	Outer rotating cylinder electrode (ORCE)
Cathode surface (cm^2)	21	452	69
Anode surface (cm^2)	21	615	24
Anode/cathode distance (cm)	1	1	2
Electrolyte volume (l)	2	6	0.6
Flow-rate or rotation rate	1–400 l h^{-1}	80–230 rpm	300 rpm
Connection type	Bolt	Brushes	Brushes

The first configuration was a horizontal parallel plates (PP) cell, in which the electrolyte medium was circulated between two horizontal electrodes: the cathode at the bottom and the anode at the top. This circulation rate was controlled by means of a centrifugal pump, a perfectly mixed storage tank and a magnetic flow meter. The flow rates ranged from 1 to 400 L h^{-1}, the hydraulic diameter being 1.8 cm. The storage tank atmosphere of the reactor was kept under slight overpressure by a continuous nitrogen stream that allows removal of the electrochemically produced gases. A Tacussel PRT10-20X potentiostat was used for galvanostatic operations.

The second device was an inner rotating cylinder electrode (IRCE) cell. A batch reactor contained the electrolyte

and the electrodes. The cathode was a rotating cylinder surrounded by the anode in an axisymmetric configuration, being slightly larger to ensure homogeneous current distributions.

The third cell configuration was an outer rotating cylinder electrode (ORCE) cell, what is less common for electrodeposition. The cathode was an outer rotating cylinder and the anode, located at the center of the reactor (axisymmetric configuration), was a motionless nickel cylinder.

A rectifier 0-100 A (Acore RGT 172) has been used for both I and ORCE devices.

2.2 Materials

Solutions were made from NaOH Flakes (min. 97% Pur.) dissolved in purified water (MilliQ) to obtain a 50 wt% NaOH–H_2O electrolyte. The density and viscosity of the electrolyte in such conditions have been evaluated at 1460 kg m^{-3} [9] and 2.3 × 10^{-3} Pa s respectively [10]. Hematite particles were from VWR, with purity above 85%. Their bulk density was taken as 5260 kg m^{-3} [11]. Measurement of their particle size distribution with a Malvern Mastersizer type S revealed one peak centered at 0.4 μm and a larger one at 10 μm. The concentration in particles in standard conditions was 33 wt% (13 vol%) and conversion during electrolysis experiments was less than 2%, except for the ORCE configuration in which conversions up to 40% could be attained.

Temperature was kept between 100 and 110 °C by circulation of warm oil or use of an electrical resistance surrounding a thoroughly stirred vessel for suspension homogenization: the vessel acted as the electrochemical cell in the case of cylindrical electrodes or was the ancillary device with the PP electrode cell.

Cell material was 316L stainless steel, except for the ORCE cell which was made out of PTFE. The anode material was 99% nickel, and the cathode material was low porosity graphite in PP and IRCE configurations, and mild steel for the ORCE.

2.3 Observations and analysis

Scanning Electron Microscopy (SEM) observations were made using a JEOL JSM-840 apparatus with a 15 keV beam. After observation, iron deposits were submitted to weight measurement to evaluate the faradaic yield, taking into account the cell current and the duration of the runs. The amount of metal contained in such weighted deposits has been validated thanks to analysis by X-rays diffraction, chemical analysis, and Mössbauer spectroscopy: all of them had a Fe-metal content higher than 91%.

3 Results

3.1 Faradaic efficiency

Faradaic efficiency is defined as the ratio between the recovered deposit weight and the theoretical weight of metal calculated from the overall electrical charge after galvanostatic run using Faraday's law following reaction (1).

$$Fe_2O_3 + 3H_2O + 6e^- \rightarrow 2Fe + 6OH^- \quad (1)$$

The anode reaction is:

$$6OH^- \rightarrow \frac{3}{2}O_2 + 3H_2O + 6e^- \quad (2)$$

The thermodynamical cell voltage was evaluated for the temperature and concentration conditions of interest at 1.24 V [12].

A current density of 0.1 A cm^{-2} has been used with the three cells under study. Based on a conventional chemical engineering approach, the dimensionless Sherwood number, describing the contribution of diffusive transfer phenomena and evaluated from available correlations (cf. Appendix), has been used for each configuration. Corresponding mass transfer coefficients have been calculated assuming a diffusion coefficient of the reacting species of 10^{-9} m^2 s^{-1}, the order of magnitude of ions diffusivity in alkaline electrolyte [2]. This method provides a first basis for comparison of the various configurations, all the operating parameters e.g., electrolyte, temperature, particle size, and concentration (ions, solid particles) being kept equal. It can be stressed that we neglect in this approach the role of suspended particles on the enhancement of mass transfer rates: the presence of solids could enhance the transfer rates by a factor ranging from 2 to 6 [13–15] or of the effect induced by the electrogenerated gas. Operating conditions allowing high faradaic efficiencies to be obtained, mentioned in the experimental sections and the caption of Fig. 2, have been determined by searching suitable velocity of the electrolyte media or of the electrode for postulated current values of the order of 0.1 A cm^{-2}: the optimal temperature and the concentrations of both electrolyte and suspended particles had been formerly determined [16]. These conditions related to both chemical and hydrodynamic aspects are referred to as "standard operating conditions" hereafter.

The efficiency is above 0.8 for all configurations, whatever the rate of diffusive convection transfer, in agreement with previous results on suspension electrolysis [5, 7]. The faradaic efficiency was observed to be lower for the configurations which provide the higher mass transfer rate (IRCE and ORCE), and the best results have been obtained in the PP configuration with current yields up to 98%. For a given configuration, the efficiency is reduced

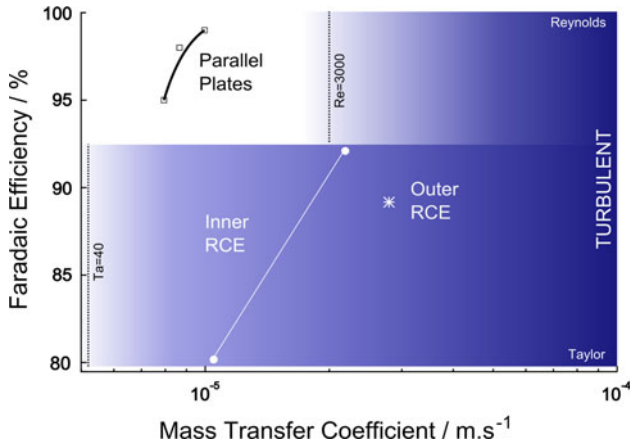

Fig. 2 Variation of the faradaic efficiency for iron deposition on the three tested-configurations at 0.1 A cm^{-2}. Theoretical deposit thicknesses were 144, 290, and 578 μm for PP, IRCE, and ORCE devices, respectively. Maximum Reynolds number is 2200 for PP, with Taylor numbers being 230 and 430, respectively, for IRCE and ORCE. *Grey areas* represent transition to the turbulent regime in both configurations

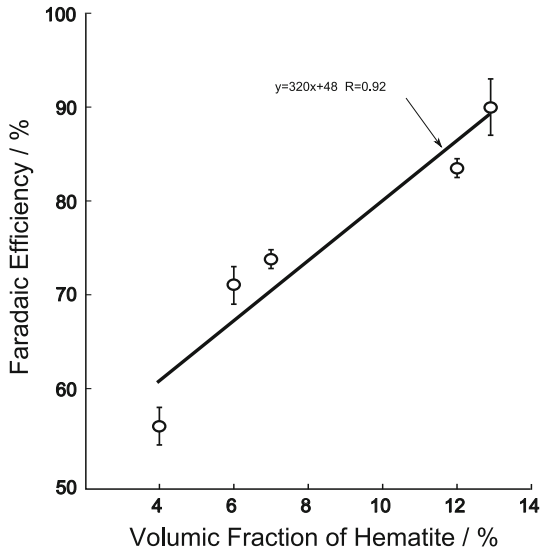

Fig. 3 Influence of the hematite concentration on the faradaic efficiency for iron deposition in the PP configuration (theoretical thickness = 97 μm, velocity 0.14 m s^{-1}, $Re = 1600$, $k_L = 8.9 \times 10^{-6}$ m s^{-1} and current density 0.1 A cm^{-2})

by lower mass transfer rates, in agreement with the usual engineering rules: lower transfer rates of the reactants are to limit the overall reduction to iron, then favoring side reaction, in this case hydrogen evolution.

These results, therefore, suggest a contribution of flow conditions in the reactor on the iron metal production rate. Assuming that the reactive species are trivalent iron ions, the limiting current density is calculated as

$$j^{\lim}_{\mathrm{Fe+III}} = 3F \cdot C_{\mathrm{Fe+III}}\, k_{\mathrm{L}}$$

Considering the solubility value of Fe(III) in the electrolyte solution at 2.6×10^{-3} mol L^{-1} at 110 °C [2], this limiting current density is in the range $[0.75–2.07] \times 10^{-3}$ A cm^{-2}, which is far below the applied current density. This confirms that iron deposition does not obey the conventional diffusive transfer limitation of dissolved species.

Moreover, the influence of the concentration of hematite has been studied in the case of the PP configuration, as presented in Fig. 3. Hematite concentration has an important effect on the faradaic efficiency which could correspond, in the specific configuration studied, to a limitation of the iron metal deposition by mass-transfer phenomena. Nevertheless, it has to be noticed that the deposit morphology is affected by particle concentration: powdery, brittle deposits were produced with low particle concentrations, most likely resulting from appreciable side hydrogen evolution. For such cases, the metal losses induced by mechanical abrasion of the electrode surface by the flowing suspension leads to lower amounts of metal recovered at the end of the run, further to underestimates of the deposition current yield. The role of the particle concentration could, therefore, not be directly described by a simple concentration/limiting current relationship. The difference observed between the various configurations can only be analyzed through evaluation of particle trajectory in the cells.

A study of the reaction faradaic efficiency for the IRCE has been conducted to establish the influence of both the electrolysis time and the possible accumulation of intermediate species on the cathode surface during the process. The electrolysis has been run in one 3-h batch and the results are compared on Fig. 4 with three successive 1-h runs of one hour, with recovery of the metal deposited after each of them. It must be mentioned that foam has been observed on the cathode surface and in the liquid bulk immediately at the reactor opening.

The faradaic efficiency is 10% higher after three successive 1-h runs with intermediate recovery of the deposit than for a 3-h batch process. The efficiency of the deposition process in such configuration, therefore, appears to decrease along the electrodeposition process.

3.2 Morphology of the deposits

Figure 5 presents macroscopic views of the deposits produced on the various configurations for the conditions of Fig. 2. The deposit produced on the horizontal PP cell does not exhibit strong adhesion on the cathode and is fairly brittle. The moderate thickness of the deposit (144 μm) may be the cause of its poor mechanical cohesion properties. Typical SEM views of samples produced with the PP configuration are presented in Fig. 6. As shown in Fig. 6a, the deposit roughness is pronounced with metal nodules

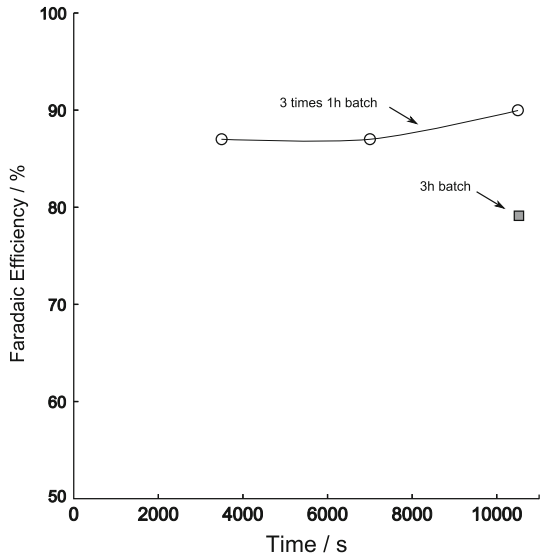

Fig. 4 Variation of the faradaic efficiency for one 3-h batch (theoretical thickness 289 μm), and three successive runs of 1 h in the IRCE device (theoretical thickness = 96 μm, 80 rpm, k_L = 1.71×10^{-5} m s^{-1} and current density 0.1 A cm^{-2})

being of 50–80 μm in diameter. This roughness is however only a surface effect as seen in the cross-section view (Fig. 6b) where relatively low porosity is noticed: it was estimated below 10% by using image analysis technique. The crystal morphology (Fig. 6c) is characteristic of iron metal deposit in alkaline media [2, 7] and does not exhibit any shape-feature from the original iron oxide particles.

The deposit obtained on the IRCE surface is very uniform and fairly adherent. Figure 7 gives typical SEM observations of deposits produced with the IRCE configuration. The surface also exhibits a nodular aspect, however, with larger nodules: each of them being 100 μm large, lying close to its neighbours. The deposit is, therefore, very compact, as confirmed by cross-sectional observations (Fig. 7d) whose image analysis yields porosity estimate below 5%. This is in accordance with longer-term deposition in similar configuration, for which porosity was shown to be below 5% [17]. Altogether, the deposit obtained from iron oxide suspension electrolysis, therefore, share some features of those obtained for other metals in conventional metal electrodeposition processes. At the grain size scale (around 10 μm), crystallites are larger and their arrangement very compact (Fig. 7c).

The deposit on the ORCE is less uniform, with pronounced edge effects at its bottom. Figure 8 reports SEM views of deposit obtained in the ORCE configuration. The non-uniform aspect already observed on

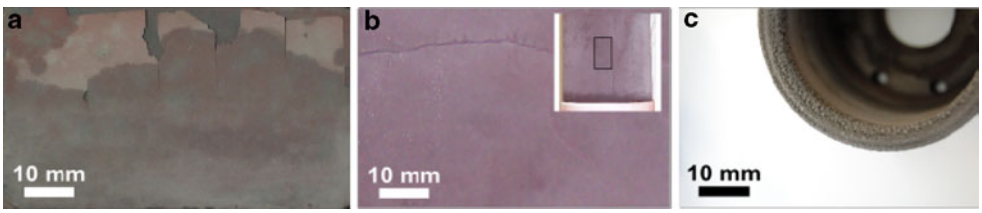

Fig. 5 Macroscopic views of deposits. **a** PP (whole surface), **b** inner RCE (*inset*: overall surface), and **c** outer RCE (cathode view upside down). (Standard operating conditions—deposits obtained for conditions of Fig. 2)

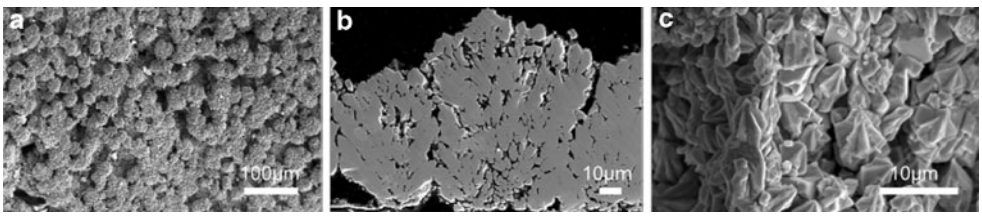

Fig. 6 SEM views of the surface (**a**, **c**) and cross-section (**b**) of deposit produced on the parallel plates configuration (standard operating conditions)

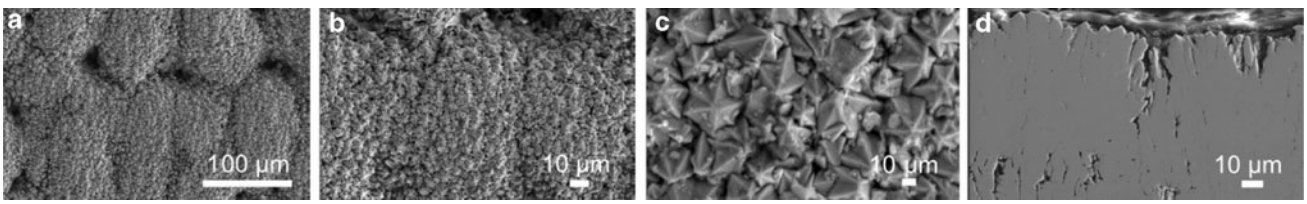

Fig. 7 SEM observations of surface (**a**–**c**) and cross-section (**d**, partial view) of deposit obtained on Inner RCE configuration (standard operating conditions)

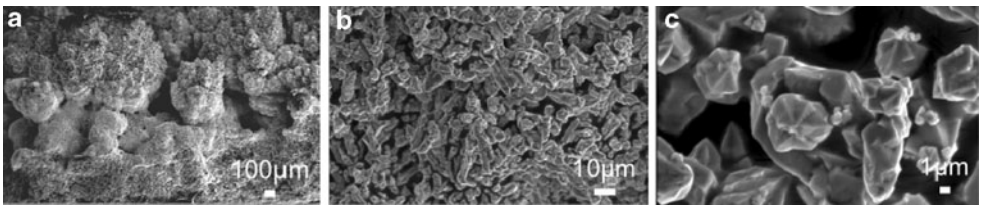

Fig. 8 SEM views of the surface of deposit produced on the ORCE (standard operating conditions)

macroscopic views is confirmed at the micrometer scale (Fig. 8a). This differs quite a lot from the observations made with PP and IRCE configurations: this difference may be due to the centrifugal force, which tends to project particles onto the cathode surface, leading to possible accumulation and shielding of the electrically active surface by the local higher resistivity. Nevertheless, at higher magnification, the grains structure and size are comparable to those observed with the other deposition devices (Fig. 8c).

3.3 Cell voltage

Referring to typical electrowinning processes, the gap used in the developed configurations (between 1 and 2 cm for all of them) is very small for the fairly high current densities foreseen for the process. The conductivity of such highly concentrated electrolyte at high temperature is evaluated to 120 Ω^{-1} m^{-1} from available data for alkaline solution at the operating temperature (150 Ω^{-1} m^{-1}) [18, 19] and using Bruggeman relation, taking into account the volume concentration in hematite particles at 13%. The ohmic drop per meter of gap at 1000 A m^{-2} is approx. equal to 8.33 V m^{-1}, which corresponds to 83.3 mV for 1 cm gap cell.

An example of the time variation of the cell voltage in the PP configuration is presented in Fig. 9, where the variation of the flow-rate and the temperature of the electrolyte are also reported. Around 2000 s are required to reach the desired temperature of 100 °C, above which the cell voltage, the temperature, and the flow rate attain steady-state levels. The cell voltage is much lower than for the other configurations, with a remarkably low value of 1.66 V, stable during the electrolysis process. This can be converted to electrical energy consumption in the cell near 2800 kWh t_{Fe}^{-1}, assuming a faradaic efficiency of 0.9 as indicated by the experiments shown above.

Experiments conducted with IRCE and ORCE configuration lead to cell voltages higher than 2 V (data not shown). In both cases, the measured voltage is largely increased by the insufficient efficiency of shaft/current feeder contact consisting of four graphite brushes rubbing against the shaft. The increase of cell voltage is, therefore, not primarily due to higher electrode overpotentials and ohmic drop between the electrodes.

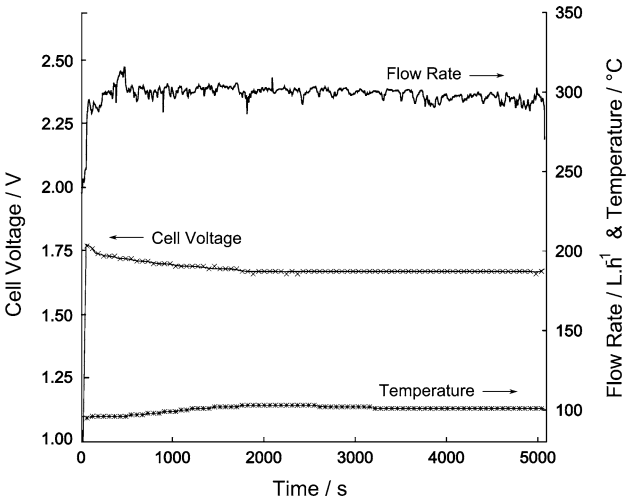

Fig. 9 Cell voltage (*left axis*), temperature and flow-rate (*right axis*) variation during typical galvanostatic run at 0.1 A cm^{-2} on the parallel plates configuration

4 Discussion

The experimental results obtained on three very different electrolysis cells reveal that the suspension electrolysis process can be easily conducted with high current efficiency in various cell configurations, in agreement with previous small scale studies. More interestingly for electrochemical engineers, these results are particularly useful to study the transfer phenomena involved in the process. They confirm that the conventional diffusion/convective mass-transfer rates of soluble Fe(III) species is not sufficient to predict reactor production rates for the suspension process under study. More precisely, the faradaic efficiency, the deposit morphology, and properties, together with the results of cell voltage measurement results show that two complex multiphase transport processes must be properly understood to run efficiently the alkaline iron electrowinning process, namely (i) the flow of suspended particles in the electrode gap, and (ii) the motion of the

electrogenerated gas in the flowing medium. Solving these two phenomena with suitable technological solutions is of crucial importance to guarantee minimum energy losses of the electrolysis process.

4.1 The cathodic reaction of solid particles in suspension: a new approach of electrochemical engineering

The cathode reaction of metal deposition is probably the most important phenomenon for electrolytic iron production. Solid particles must be transferred to the cathode surface to guarantee high faradaic efficiency of the process. This transfer, because of the size of the particles does not obey to simple diffusion, since micrometer sized hematite particles would have a Stokes–Einstein diffusivity near 10^{-14} m^2 s^{-1} in the alkaline electrolyte at 100 °C. However, hematite particles are too small to follow a trajectory entirely governed by gravity in convection-free conditions, since their single terminal velocity is 8×10^{-5} m s^{-1}, with a corresponding Reynolds number of the particle near 0.05.

More precisely, the study of the different configurations helps to identify the important role of gravity and other mechanical forces on the particles transfer. As a matter of fact, the IRCE configuration appears detrimental to faradaic efficiency, especially for long-term electrolysis, while the ORCE is fairly efficient for large conversion of feed particles, i.e., up to 40% within one batch run. The centrifugal force is undoubtedly involved in both rotating configurations, being a favorable phenomenon for the ORCE, but exhibiting a detrimental effect in the IRCE. The role of gravity is stressed by the good results obtained with the PP configuration with the facing up cathode at the bottom. However, it is also observed that the porosity of the deposits is more important in configurations where accumulation of particles occurs: deposits in the PP cell are fairly porous with a high roughness while those produced in the IRCE are very compact. Interestingly, the use of less concentrated suspensions in the PP configuration leads to more porous deposits produced with lower current efficiency. This is to be related to the enhanced sedimentation of less concentrated suspensions as predicted by Richardson and Zaki's law [20] for a suspension of uniform particles at volumic fraction Φ, which evaluates the sedimentation velocity u_{t_s} through:

$$u_{t_s} = u_{t_0}(1-\phi)^{4.65}$$

We can, therefore, conclude that accumulation of particles is detrimental to the deposit compactness. This observation can be explained by the electrical insulating role of too thick layer of little-conducting hematite particles at the cathode surface. This is important for large scale development of the process where handling of metal deposit is necessary, an operation more easily carried out with deposits of sufficient compactness and mechanical resistance. A compromise between particles transfer and departure rates, and sufficient contact time at the cathode is required to enable homogeneous growth of the metal together with high faradaic efficiency. As observed in rotating-disk experiments, where current densities higher than 15,000 A m^{-2} have been obtained [7], the current efficiency issue is not strongly related to the applied current density provided particles cover the cathode surface. This process feature is related to the large amount of Fe^{III} reactant supplied by each 10-μm transported particle [3]. The method to run the process with high efficiency is then directly related to the control of the suspension flow and the corresponding solid/liquid interactions.

Considering flow phenomena of suspended particles, a chart can be built to evaluate the conditions for which particle's own trajectory must be taken into account, as shown by calculation of the Stokes number for 10-μm hematite particles depending on the characteristic length (Fig. 10).

$$Sk = \frac{\rho_P \cdot d_p^2 \cdot u_L}{\mu_L \cdot L}$$

The minimum relevant characteristic flow length, L, can be the average free distance of a particle between two collisions with another in the concentrated swarm, or an

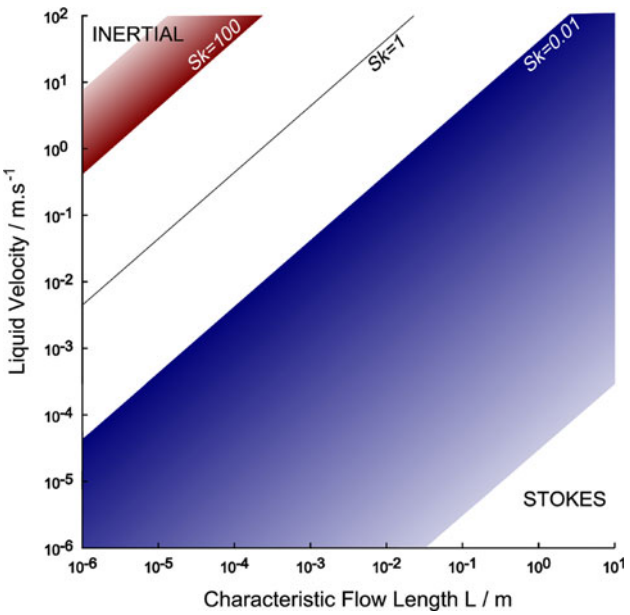

Fig. 10 Flow regime map for 10-μm hematite particles in alkaline electrolyte. Boundaries have been drawn for Stokes number above 100 (on top, inertia regime) and lower than 10^{-2} corresponding to Stokes regime

estimate for the diffusional layer of the Nernst model, or eventually the Kolmogoroff scale. In this case, because of the flow regime and the particle dimensions, typical value for L can be taken at 10 μm. For $L = 10^{-5}$ m, hematite particles have appreciable inertia for liquid velocity over 1 m s^{-1}. In contrast for liquid velocity below 1 mm s^{-1}, the particles follow perfectly the liquid stream. As concerns velocity, one can hardly consider a large scale process with liquid velocity far larger than 1 m s^{-1}, because of the significant energy consumptions involved. The suspension process will then be run in conditions where the particles behavior is less inertial, more of Stokes-type, i.e., for which particles follow more the liquid streamlines.

The engineering issue is then related to suspension flow in reactor, and more precisely to the difficulty in avoiding accumulation of particles on the cathode surface by settling.

This study has shown that although these conditions cannot easily be predicted, they can practically be fulfilled in various electrolysis cell configurations. The horizontal one is subjected to particle's accumulation, and very sensitive to the suspension concentration. The vertical configurations must be carefully designed, taking the role of centrifugal forces into account in the accumulation of solid particles. The selection amongst these configurations considering solely the cathode reaction is, therefore, not sufficient, since the presence of the generated gas by the anodic reaction has also to be considered in the selection of the process.

4.2 The gas evolution reaction: a key parameter to reach energetic efficiency

The study of several cell configurations evidenced an important aspect of the process: the oxygen gas produced on the anode requires a dedicated configuration for its efficient removal from the electrode gap, thus for low energy consumption. Indeed, the IRCE configuration exhibits a limitation in the faradaic efficiency with longer electrolysis times and deposit thickness. The approach made for particle transport and flow upon the action of gravity/centrifugal forces can be applied to the oxygen bubbles produced at the anode: their low density with respect to the suspension (3 orders of magnitude below) allow them to be dragged toward the rotating surface, i.e., the cathode, where they can react and limit the efficiency [21]. This provides a qualitative explanation of results presented in Fig. 4, where interruption of the electrolytic run and recovery of the metal produced allows significant degassing of the reactor liquid. On top of this, the side-reduction of oxygen is far more efficient on iron metal than on graphite, which can explain the higher efficiency obtained for small deposit thickness.

As a matter of fact, the two other configurations are more efficient, partly because the gas phase is maintained far from the cathode. The mechanical forces have a positive effect in the ORCE cell, with centripetal trajectory of the light phase toward the anode. In the PP configuration, the buoyancy is sufficient to keep the oxygen phase in the upper part of the cell in spite of the suspension flow, and so the gas can be dragged out of the cell by the electrolyte flow. The corresponding energy consumption, in terms of both faradaic efficiency and cell voltage inherited from ohmic limitation due to bubbles, is then significantly reduced.

4.3 Energy efficiency of the electrolysis process

In addition to the key mass-transfer issues previously presented, other important facts have to be discussed. First, the role of the current collecting method has been shown, as rotating contacts have proved to be the cause of appreciable ohmic losses in high current systems. This is consistent with existing technology for large-scale production of metal e.g., aluminum, copper, or zinc, where no electrodes are in movement: simple, reliable, and thrifty techniques for current leads have to be used. In terms of energy needs, it needs, indeed, to be emphasized that 10-mV loss in electrical contacts corresponds to 16 kWh t_{Fe}^{-1} for 90% faradaic efficiency. In spite of the possible beneficial effect of centrifugal forces in the ORCE cell, the energy consumption of the rotating engine, together with the required current lead technology, renders this configuration hardly suitable for large scale production.

The results obtained with the PP configuration are both promising and meaningful: the efficient gravity-based separation of cathodic reactant and anodic products lead to a high current efficiency and a low electrical energy consumption. This result is a breakthrough for electrowinning of a multiple valency metal: iron metal has been electrowon from iron oxide in industrially relevant configurations without using a diaphragm. The iron metal is then seen as a metal which could be produced at large scale by electricity without CO_2 production at the anode: contrary to graphite, nickel anodes are inert and exhibit appreciable electrocatalytic properties for oxygen evolution reaction, which is to result in lower cell voltage and energy consumption.

5 Conclusion

Iron electrowinning from alkaline suspensions of hematite particles has been conducted in three typical electrolysis cell configurations with very promising results. The various

hydrodynamics conditions studied reveal that the mass-transfer limitation is not of the diffusive type, and that gravity is a key force to reckon with in the design of a dedicated electrolysis cell. The horizontal PP configurations is the most promising configuration with energy consumption lower than 3000 kWh t_{Fe}^{-1}, for production of compact iron metal plates. This value must be corrected for the cost of a preprocessing step of iron ore grinding and a melting step, leading to total energy needs at around 3600 kWh t_{Fe}^{-1} (i.e., 13 GJ t^{-1}) a value potentially lower than present most-efficient full route based on the blast-furnace [22]. These results stress that the low-temperature electrolysis technology is a potential method to produce steel with very low CO_2 emission, provided C-lean electricity is used.

Acknowledgements This study has received financial support from the ULCOS program, which operates with direct financing from its 48 partners, especially of its core members (ArcelorMittal, Corus, TKS, Riva, Voestalpine, LKAB, Saarstahl, Dillinger Hütte, SSAB, Ruukki and Statoil), and has received grants from the European Commission under the 6th Framework RTD program and the RFCS program (priority 3 of the 6th Framework Programme in the area of "Very low CO_2 Steel Processes", in co-ordination with the 2003 and 2004 calls of the Research Fund for Coal and Steel). Authors wish to thank staff of the mechanical workshop of LRGP & ArcelorMittal Maizières for their technical performances. AA would like to thank A. Vandeix, D. Lefevre, E. Perspicace, and J. M. de Oliveira for their contribution to the experiments.

Appendix: Estimation of mass transfer coefficient in the cells

For the PP configuration, the Reynolds number of the liquid was calculated as per the following equation:

$$Re = \frac{u_{av} d_h}{v} \tag{3}$$

where u_{av} is the average velocity of the medium, v its kinematic viscosity, and d_h the hydraulic diameter in the rectangular channel. The kinematic viscosity of the medium was taken as equal to one of the particle-free NaOH solution at 100 °C, at 1.58×10^{-6} m^2 s^{-1}. For liquid flow rates ranging from 1 to 400 L h^{-1}, Re varies from 6.35 to 2540. The flow was, therefore, considered as fully laminar for estimation of the mass transfer coefficient, k_L: Lévèque's relation was employed for this purpose:

$$Sh = \frac{k_L \cdot d_h}{D} = 1.85\left(Re \cdot Sc \frac{d_h}{L}\right)^{1/3} \tag{4}$$

where L is the length of the cell, here equal to 7 cm, Sc the Schmidt number (= v/D) and D the diffusion coefficient of the electroactive species: D was taken at 10^{-9} m^2 s^{-1}, considering the reaction of ionic species only. For the considered conditions, k_L varied from 1.41×10^{-6} to 1.04×10^{-5} m s^{-1}.

For the IRCE configuration, Taylor number, Ta, was calculated to characterize flow conditions:

$$Ta = \frac{R_i^{1/2} \Omega_i (R_o - R_i)^{3/2}}{v} \tag{5}$$

where R_o and R_i are the radius of the external and internal cylinders, respectively, and Ω_i the angular velocity of the internal cylinder (in rad s^{-1}). Ta was higher than 400 in all cases and Eisenberg's correlation [23] could then be employed:

$$k_L = 0.0791 Re_w^{-0.3} (\Omega_i R_i) \cdot Sc^{-0.644} \tag{6}$$

where Re_w is defined as:

$$Re_w = \frac{2R_i^2}{v} \tag{7}$$

For rotation rates of the inner cylinder of 80 and 230 rpm, the mass transfer coefficient was estimated at 1.46×10^{-5} and 3.06×10^{-5} m s^{-1}, respectively. For the ORCE cell, Kreith's correlation [24] was used:

$$Sh_D = \frac{(2R_o)k_L}{D} = 0.18\left(0.5 Sc \cdot Re_D^2\right) \tag{8}$$

where Re_D is defined as

$$Re_D = \frac{(2R_o)^2 \Omega_o}{v} \tag{9}$$

where Ω_o is the angular velocity of the external cylinder in rad s^{-1}. When the cylinder is rotating at 300 rpm, mass transfer coefficient is equal to 2.75×10^{-5} m s^{-1}.

References

1. Birat J-P, Borlée J, Korthas B et al (2008) SCANMET III, the ULCOS program: a progress report in the Spring of 2008. In: 3rd international conference on process development in iron and steelmaking, Luleå, Sweden, http://www.scanmet.info
2. Allanore A, Lavelaine H, Valentin G et al (2007) J Electrochem Soc 154:187
3. Allanore A, Lavelaine H, Valentin G et al (2008) J Electrochem Soc 155:125
4. Lloyd SJ (1929) Trans Am Electrochem Soc 55:305
5. Leduc JAM, Loftfield RE, Vaaler LE (1959) J Electrochem Soc 106:659
6. Allanore A, Feng J, Lavelaine H et al (2010) J Electrochem Soc 157:24
7. Juan BY, Kongstein OE, Haarberg GM (2009) J Electrochem Soc 156:64
8. Pickett DJ (1977) Electrochemical reactor design. Elsevier Scientific Publishing Company, NY
9. Krey J (1972) Z Phys Chem 81:252
10. Klochko MA, Godneva MM (1959) Russ J Inorg Chem 4:964
11. Cornell RM, Schwetmann U (2003) The iron oxide—structure, properties, occurrences and uses. Wiley-VCH, Weinheim

12. Beverskog B, Puigdomenech I (1996) Corros Sci 38:2121
13. Kwon SG, Doh DS (1989) Int Chem Eng 29:255
14. Deslouis C, Ezzidi A, Tribollet B (1991) J Appl Electrochem 21:1081
15. Stankovic VD (1994) J. Appl Electrochem 24:525
16. Elias J (1994) Master thesis, Institut National Polytechnique de Toulouse LGC-UPS
17. Allanore A (2007) PhD dissertation, Institut National Polytechnique de Lorraine, ENSIC-LSGC, France. Available at http://tel.archives-ouvertes.fr/tel-00341283/fr
18. Krings W (1948) Z Anorg Chem 255:194
19. Krings W (1952) Z Phys Chem (N F) 81:252
20. Richardson JF, Zaki WN (1954) Trans Inst Chem Eng 32:35
21. St-Pierre J, Massé N, Bergeron M (1995) Electrochim Acta 40:1013
22. De Beer J, Worell E, Blok K (1998) Annu Rev Energy Environ 23:123
23. Eisenberg M, Tobias CW, Wilke CR (1954) J Electrochem Soc 101:306
24. Kreith F (1968) Adv Heat Transf 5:129